Proton propagation in nuclei studied in the $(e,e'p)$ reaction

G. Garino,[a] M. Saber,[b] and R. E. Segel
Northwestern University, Evanston, Illinois 60208

D. F. Geesaman, R. Gilman,[c] M. C. Green,[d] R. J. Holt, J. P. Schiffer, and B. Zeidman
Argonne National Laboratory, Argonne, Illinois 60439

E. J. Beise,[e] G. W. Dodson, S. Høibråten,[f] L. D. Pham,[g] R. P. Redwine, W. W. Sapp, C. F. Williamson, and S. A. Wood[h]
Massachusetts Institute of Technology, Cambridge, Massachusetts 02139

N. S. Chant and P. G. Roos
University of Maryland, College Park, Maryland 20742

J. D. Silk[i]
University of Pennsylvania, Philadelphia, Pennsylvania 19104

M. Deady[j]
Mount Holyoke College, South Hadley, Massachusetts 01075

X. K. Maruyama[k]
National Institute for Standards and Technology, Gaithersburg, Maryland 20899
(Received 10 October 1991)

Proton propagation in nuclei was studied using the $(e,e'p)$ reaction in the quasifree region. The coincidence $(e,e'p)$ cross sections were measured at an electron angle of 50.4° and proton angles of 50.1°, 58.2°, 67.9°, and 72.9° for ^{12}C, ^{27}Al, ^{58}Ni, and ^{181}Ta targets at a beam energy of 779.5 MeV. The average outgoing proton energy was 180 MeV. The ratio of the $(e,e'p)$ yield to the simultaneously measured (e,e') yield was compared to that calculated in the plane-wave impulse approximation and an experimental transmission defined. These experimental transmissions are considerably larger (a factor of ~2 for ^{181}Ta) than those one would calculate from the free N-N cross sections folded into the nuclear density distribution. A new calculation that includes medium effects (N-N correlations, density dependence of the N-N cross sections and Pauli suppression) accounts for this increase.

PACS number(s): 25.30.Fj, 24.90.+d

I. INTRODUCTION

An understanding of nucleon propagation in nuclei is of fundamental importance and also necessary in the interpretation of nuclear experiments where nucleons are detected. Such propagation has often been characterized in terms of a mean free path (λ), the average distance between collisions. The simplest model of the mean free path [1,2], $\lambda=1/\rho\sigma$ with a correction for Pauli blocking, yields for a proton energy of 180 MeV a value of ~2.4 fm at nuclear matter density ($\rho_{\rm NM}=0.16$ fm^{-3}) using the isospin-averaged free nucleon-nucleon (N-N) cross section σ. A mean free path (MFP) may also be obtained through the use of an optical-model potential (OMP), which describes the nucleon propagation in terms of a complex potential:

$$\lambda(r)=\frac{\sqrt{\hbar^2[E-V(r)]/2m}}{W(r)}\ , \tag{1}$$

where $V(r)$ and $W(r)$ are the real and imaginary potentials, respectively, m is the nucleon mass, and E is the ki-

[a]Present address: University of Illinois, Champaign, IL 61820.
[b]Present address: King Faisal University, Dammam, Saudi Arabia.
[c]Present address: Rutgers University, New Brunswick, NJ 08855.
[d]Present address: LeCroy Research Systems, Spring Valley, NY 10977.
[e]Present address: California Institute of Technology, Pasadena, CA 91125.
[f]Present address: University of Colorado, Boulder, CO 80309.
[g]Present address: Exxon Production Research, Houston, TX 77252.
[h]Present address: CEBAF, Newport News, VA 23606.
[i]Present address: Institute for Defense Analyses, Alexandria, VA 22311.
[j]Present address: Bard College, Annandale-on-Hudson, NY 12504.
[k]Present address: Naval Postgraduate School, Monterey, CA 93943.

netic energy of the nucleon.

Many determinations [3] of the phenomenological OMP in the 100–200 MeV regime have been made by fitting to proton elastic-scattering data; any excitation of the target nucleus is considered absorption. These analyses typically employ a local OMP with real and imaginary central and spin-orbit potentials. The radial shapes of the central potentials are given by the usual Woods-Saxon form. Such fits yield values of λ of the order of 5–7 fm in the energy range 150–200 MeV. Meyer and Schwandt [4] have shown for ^{40}Ca(p,p) that a modified real central potential shape, with a depressed central region (the so-called "wine-bottle" shape) requires a deeper imaginary potential to fit the data, corresponding to a MFP in the range 1.5–3 fm.

The OMP is derived from N-N interactions [5] and is nonlocal [6]. Several authors [7,8] have pointed out the importance of the nonlocality inherent in nuclear matter when discussing the mean free path and obtain $\lambda \sim 4$ fm [7,8] in the energy range 150–200 MeV.

Classical analyses of both proton quasifree scattering—(p,p') and $(p,2p)$—and proton total and reaction cross sections yield values of the MFP of 2.5–3.5 fm [9,10] for 150–200 MeV protons. Schiffer [11] first pointed out the lack of agreement between these values, the optical potential results and the theoretical expectations. Given this range in values of the MFP, a more direct measure of the proton attenuation is desirable.

In the present work, the attenuation of the proton in the nucleus has been studied by examining the A dependence of the $(e,e'p)$ reaction. An electromagnetic probe has important advantages over a hadronic probe, because (1) the distortion of the incident electron is small, (2) only one proton is involved in $(e,e'p)$ and it is the attenuation of this proton that is measured, and (3) the virtual photon illuminates the entire nuclear volume. Proton elastic scattering in this energy range is less sensitive to the nuclear interior [12]. Since the whole nucleus is illuminated by the virtual photon in the $(e,e'p)$ reaction, the macroscopic nuclear transmission is more directly measured.

Two distinct but related concepts are important in describing proton attenuation. The first is the elastic or optical model description discussed above where any interaction removes flux from the reaction channel. However, experimentally at energies ≥ 100 MeV it is more straightforward, and often more relevant, to consider a macroscopic attenuation where small losses in energy or changes in angle by the proton are not considered as a loss of flux. It is this macroscopic attenuation which is often required to interpret reaction data with protons in the entrance or exit channel.

II. EXPERIMENT

The ratio of $(e,e'p)$ coincidence yield to (e,e') singles yield was measured in the quasifree region at four proton angles for targets with $A = 12$–181. In the quasifree scattering process, the internal motion of the bound nucleon is expected to spread the ejected nucleons over a cone with a half angle of $\theta_F = \tan^{-1}(k_F/|\mathbf{q}|) \sim 22°$ for this experiment, where $\mathbf{q}$ is the three-momentum transfer of the virtual photon and k_F is the Fermi momentum. The proton detector was placed at four angles to sample the yield over this cone. The protons had kinetic energies of 180 ± 50 MeV and the momentum acceptance of the proton spectrometer allowed detection of protons from both loosely and deeply bound orbitals.

The experiment was conducted at the Bates Linear Accelerator Center where 779.5 ± 3.1 MeV electrons were scattered by ^{12}C, ^{27}Al, ^{58}Ni, and ^{181}Ta targets. A detailed description of the experimental procedure and the data analysis may be found in Ref. [13]. The scattered electrons were detected at the center of the quasifree peak (545–585 MeV) by the OHIPS spectrometer at an angle of $50.4° \pm 0.6°$, corresponding to $|\mathbf{q}| \sim 610$ MeV/c. Protons were detected at four angles, $50.1° \pm 0.2°$, $58.2° \pm 0.2°$, $67.9° \pm 0.2°$, and $72.9° \pm 0.2°$, by the BIGBITE spectrometer. An electron, scattering at an angle of 50.4° from a free proton, produces an outgoing proton at 49.3°. The OHIPS and BIGBITE spectrometers were mounted on a common pivot point located beneath the target chamber on beam line B. The targets were held in a movable ladder and could be changed remotely. The target ladder contained carbon, aluminum, nickel and tantalum foils of thickness ~ 100 mg/cm^2, a CH_2 (~ 50 mg/cm^2) target (rotated to distribute heat), a thin (~ 10 mg/cm^2) carbon target for calibration, and a BeO target for beam tuning. The target thicknesses were determined by weight. The background with no target was negligible.

This was the first experiment to use the BIGBITE spectrometer in its standard configuration. BIGBITE is a quadrupole-quadrupole-dipole (QQD) spectrometer with a horizontal bend and a $\pm 25\%$ momentum bite. The angular acceptance as defined by an entrance collimator was an ellipse with a horizontal axis of ± 19 mrad and a vertical axis of ± 47 mrad for a geometrical solid angle of 2.8 msr. Situated beyond the dipole were two multiwire proportional chambers (MWPC) separated by 1 m, each with an x and y plane of wires, read out using the LeCroy PCOS III system. Located beyond the chambers were two arrays of scintillators. The BIGBITE trigger was a coincidence between the two scintillator arrays.

The OHIPS spectrometer was used to detect electrons. It is a QQD spectrometer with a vertical bend and with a $\pm 3.5\%$ momentum bite. A rectangular lead collimator (± 142 mrad vertical, ± 25 mrad horizontal) defined the entrance aperture to the system, but was not the limiting aperture in the vertical direction. The quadrupole polarities were configured for maximum angular acceptance in the bend (vertical) plane, a nonstandard configuration. Above the dipole was the vertical drift chamber (VDCX) [14] consisting of two planes of wires at 45° to the horizontal. The wires were read out using a delay-line system which allowed a maximum of four wires to be read from each plane; the drift times to those wires were measured. Situated above the VDCX were three scintillators, which in coincidence defined the trigger, and a Freon Čerenkov counter with a 1-m radiator.

The trigger logic provided for simultaneous measurement of the (e,e') and $(e,e'p)$ cross sections. The proton time of flight was measured by a TDC started by the

OHIPS signal and stopped by that from BIGBITE. A coincidence event occurred when there was a simultaneous OHIPS and BIGBITE trigger. "Singles" events required an OHIPS trigger without a BIGBITE trigger, and were prescaled by a factor of 50. The dead time was measured by the ratio of two scalers, one gated and the other not gated by the experiment busy signal. Two toroids were used to monitor the beam current; the two toroid measurements agreed to within 0.7%. The LAMPF Q system [15] was used both for data acquisition and for off-line analysis.

During calibration, each spectrometer operated independently. At a beam energy of 250.1±1 MeV (measured in the ELSSY [16] spectrometer), the quadrupole magnetic fields were scanned to minimize the width of the $^{12}C(e,e)$ elastic peak. The FWHM of the elastic peak was 0.5% for OHIPS, constant across the focal plane, and for BIGBITE ~1% at the center and ~2% at the edges of the focal plane. Elastic e-p scattering at 779.5 MeV in both singles and coincidence modes provided the most accurate determination of the spectrometer angles and beam energy, using conservation of energy and momentum.

The momentum acceptance of each spectrometer was determined in two ways. At the lower energy, the $^{12}C(e,e)$ elastic yield was measured as a function of spectrometer magnetic fields. At the higher energy, the quasifree region on each target was scanned with overlapping momentum bites. Small differences in the momentum acceptance were observed and the latter determination was used as the final momentum acceptance since it corresponded to the experimental conditions of the coincidence measurement.

The 250.1-MeV $^{12}C(e,e)$ elastic peak yield at $\delta=(p-p_0)/p=0$ was used to determine the solid angle of each spectrometer by normalizing to the cross section of Reuter *et al.* [17], a recent measurement of the elastic form factors at the ~1% level. The solid angles thus measured were 9.76±0.30 msr for OHIPS and 2.74±0.8 msr for BIGBITE. The uncertainties quoted are systematic errors (statistical errors are much smaller) including the uncertainty in the reference cross section, the uncertainties in the momentum and angle of the scattered electron, and uncertainties in the measurements of the detector efficiencies. The other sources of uncertainty (beyond counting statistics) as determined by repeated measurements of cross sections are estimated to be ~2%. The electron singles cross sections measured at the proton angle of 72.9° all were ~5% larger than those at the other angles. We have no explanation for this difference.

The overall constant systematic uncertainties, including this 2% contribution and the uncertainty in the solid angle determinations for the measured absolute cross sections, are estimated to be 3.7% for OHIPS and 3.5% for BIGBITE. Since the errors in the solid-angle determination are partially correlated, the uncertainty in the absolute coincidence cross sections is 6.3%. Uncertainties in the electron (OHIPS) spectrometer acceptance, beam and target normalization will, to first order, cancel in the ratio of coincidences to singles (except in the determination of the BIGBITE solid angle). Therefore, the estimated systematic uncertainty in the ratio of coincidences to singles is 3.5%.

III. DATA REDUCTION

The trajectory of a particle traversing BIGBITE was reconstructed from the measured coordinates in the two wire chambers. An event was considered to have originated in the target if the trajectory was within software-defined wire-chamber position-angle two-dimensional windows in each perpendicular direction, the limits of which were established using the elastic $^{12}C(e,e)$ dipole scan data. The efficiency of each chamber plane of BIGBITE was determined by the ratio of the number of events where there was a single hit in all planes divided by the number of events where there was a single hit in all but the plane whose efficiency was being determined. The combined efficiency of the four chamber planes was 87±1%. Events in which there were two or more clusters of hits in a single plane were recovered by eliminating those hits which did not originate in the target. Two or more hits which apparently originated from within the target were considered to be a single hit if the difference in their calculated momenta was less than 1%. Events with multiple hits that could not be recovered (approximately 5% of all real events) were discarded and were accounted for by an efficiency factor.

In OHIPS, the particle track was reconstructed from the slope and position of the trajectory in each chamber plane as determined from the measured drift times and wire positions. As in the BIGBITE analysis, a set of two-dimensional position-angle windows were defined to identify the event as originating in the target. The OHIPS analysis required that each chamber event had three or four adjacent wires hit and good drift times (both a relative and an absolute drift-time cut). The efficiencies were determined for each wire chamber and the combined efficiency of both planes was 87±1%. The efficiency of the OHIPS Čerenkov detector, determined from the scanning the $^{12}C(e,e)$ elastic peak across the focal plane, was found to be constant at 98±1% across the focal plane.

A. Radiative corrections

Radiative corrections need be applied to the experimental cross sections to obtain the lowest-order, one-photon-exchange cross section. Corrections to the elastic cross section were calculated as in Mo and Tsai [18] for $^{12}C(e,e)$.

In the continuum region, the radiative tail of the elastic peak (and other excited states) must be subtracted. The elastic radiative tail in the quasifree region was calculated as in Tsai [19] and found to be less than 0.1% of the total cross section in this region. Radiative corrections to the singles (e,e') spectra in the quasifree region were calculated as in Tsai [20] and Marchand [21]. The cross sections at lower energies required to perform the corrections were estimated using Fermi-gas calculations [22] which give a good fit to the high-energy regions of the spectra. The overall radiative corrections to the sin-

gles spectra at the center of the quasifree peak (545–585 MeV) were of the order of 5–10 %.

Radiative corrections to the coincidence $(e,e'p)$ spectra were more involved due to the additional independent variable, the missing energy E_m, since the measured missing energy changes as a result of radiation by the electron. Two approximations were made. The first was that when the electron radiates a photon of energy k_γ the missing energy is changed by k_γ regardless of whether the photon is radiated before or after the primary scattering. This approximation amounts to neglecting nuclear recoil and is good to 1% for the kinematic conditions of this experiment. Secondly, all scattered electrons were considered to have the final energy $E_e = 565$ MeV, which corresponded to the center of the OHIPS acceptance, to avoid an integration over the final electron energy. Since the corrections are at most $\pm 12\%$, these approximations introduce little error in the final results. With these assumptions, the calculation of the coincidence radiative corrections is similar to that of the singles radiative corrections and was done as in Marchand [21]. The unfolding procedure used the experimental missing energy spectra as the starting values for the iteration, and the plane-wave impulse approximation (PWIA) calculated cross sections discussed below were used to determine the missing-energy response at lower incident electron energies.

The uncertainty in the radiative correction calculation is estimated to be $\sim 5\%$ of the value of the correction. The contribution to the uncertainty of the cross section is then less than $\sim 1\%$ since the radiative corrections are $\sim 15\%$ or less. A portion of this systematic uncertainty cancels in the ratio of coincidences to singles.

IV. CROSS SECTION CALCULATIONS

In this section the various techniques for cross section calculations used in the present work are discussed. In each case it is assumed that the virtual photon interacts with only one nucleon. The general assumptions involved are the plane-wave impulse approximation (PWIA) and the distorted-wave impulse approximation (DWIA).

Frullani and Mougey [23] have reviewed the calculation of $(e,e'p)$ cross sections. The calculations here employ the so-called factorization approximation:

$$\frac{d^4\sigma}{dE_e d\Omega_e dE_p d\Omega_p} = K \sigma_{ep} S(E_s,p) , \tag{2}$$

where σ_{ep} is the off-shell electron-proton cross section, $S(E_s,p)$ is the nuclear spectral function, and K is a constant which depends on the kinematics. This factorized form for the cross section implies that the $(e,e'p)$ cross section is essentially the probability of finding a nucleon in the nucleus with separation energy E_s and momentum $\mathbf{p}$ multiplied by the cross section for scattering from such a nucleon. Model-dependent assumptions are required for each of these terms.

Since the bound nucleon is off shell (i.e., $E^2 \neq \mathbf{p}^2 + m^2$), there is some ambiguity in defining σ_{ep}. This has been discussed in detail by de Forrest [24]. The program THREEDEE [25] used for the PWIA and DWIA calculations was written for $(p,2p)$ experiments, and uses the off-shell prescriptions standard in proton scattering, termed the "initial" and "final" prescriptions. These correspond to those labeled IN and FIN in de Forrest [24] and represent the extremes of the possible choices. In the initial prescription, the incident electron and the bound proton kinematics are used in determining the cross section; in the final prescription, it is the final electron and ejected proton that are used. While there are excellent arguments suggesting better choices of the off-shell prescription, it is shown below that the primary results of this paper are not sensitive to this choice.

Two convenient parametrizations of the spectral function may be derived from a Fermi-gas distribution and single-particle distributions in Woods-Saxon potentials. A number of (e,e') experimental results have been parametrized with the Fermi-gas calculation of Moniz [22] and so these calculations have been included here only as an economical parametrization for the radiative corrections. This calculation was not used in comparing the $(e,e'p)$ coincidence and (e,e') singles data since corresponding coincidence calculations were not available.

Two single-particle parametrizations were considered for the nuclear spectral function that describes the initial nucleus. In the first, the potential confining the nucleon in the nucleus depends on the orbital it occupies and is therefore termed the "state-dependent" parametrization; in the second, the "state-independent" parametrization, each nucleon moves in the same potential. Both parametrizations were chosen to reproduce the measured binding energies of the last nucleon and the experimentally measured rms charge radii [26]. The form and parameters of the various single-particle potentials are given in Ref. [13]. The binding energies of the most deeply bound proton orbits in tantalum were 60 MeV with the state-dependent potential and 35 MeV with the state-independent potential.

The THREEDEE calculations provided a self-consistent framework for calculating singles and coincidence cross sections in PWIA and DWIA. For the singles (e,e') cross section, the PWIA is used since the attenuation of the outgoing nucleon should have a minimal effect on the singles result. Scattering from both proton and neutron orbitals contributes to the singles yield (the yield from neutrons is about 20% of the total) and an integration over the spectral function $S(E_s,\mathbf{p})$ was performed. Exclusive calculations considered scattering from protons only, since only protons are detected experimentally and charge exchange and other rescattering processes are neglected. The calculations included averaging over the angular acceptances of both spectrometers.

In the DWIA, the spectral function is replaced with the distorted spectral function $S^D(E_s,\mathbf{p}_R,\mathbf{p}')$, where $\mathbf{p}_R$ is the momentum of the recoiling nucleus and $\mathbf{p}'$ the momentum of the detected proton. The distortions of the incident and scattered electron wave are included in THREEDEE in the DWIA (but not in the PWIA) calculations by using Coulomb waves for the electron, determined by considering the nucleus to be a uniform sphere of charge.

Factorization is exact in PWIA but only approximate in DWIA. In the factorized approximation, the OMP cannot depend on the spin of the outgoing proton. The effects of the factorization approximation have been investigated by Boffi and co-workers [27] in a calculation of the $^{12}C(e,e'p)$ cross section for 500-MeV incident electrons. They found that factorization is a good approximation in parallel kinematics, but less so in perpendicular kinematics.

The inability to use a realistic optical potential with the full spin-orbit interaction makes these DWIA calculations illustrative at best. In our calculations, the central real and imaginary potentials of Nadasen *et al.* [28], obtained from a global fit to proton elastic scattering at 80–180 MeV, were used in calculating the distorted spectral function. The spin-orbit potentials of the Nadasen *et al.* potential were set to zero. This potential implies a MFP ~ 6 fm using Eq. (1).

V. EXPERIMENTAL RESULTS

A. (e,e') data

The (e,e') quasifree cross sections, as measured by the OHIPS spectrometer, are shown in Fig. 1, along with the results of the Moniz Fermi-gas calculation [22]. In this Fermi-gas calculation, the cross section was calculated for both neutrons and protons and the results added. The Fermi momentum for a given nucleon species is given by $k_F^X=(2X/A)^{1/3}k_F$, where $X=Z$ or N. The Fermi-gas parameters were fit to the high-energy end of the spectrum, where pion effects are less important. The resulting parameters are (target, k_F in MeV/c, E_B in MeV) ^{12}C, 215, 28; ^{27}Al, 234, 28; ^{58}Ni, 237, 29; ^{181}Ta, 264, 37. In general, these Fermi-gas fits to the data were relatively poor, but were only used in the radiative correction analysis; the singles radiative corrections are less than $\sim 10\%$.

The sensitivity of the PWIA calculations for nickel to the choice of off-shell cross section and single-particle distributions is illustrated along with the (e,e') data in Fig. 2. No parameters of the PWIA calculation were obtained by fitting to the data. The results indicate that the bound-state parametrization affects the shape and location of the peak, although the cross section integrated from 545 to 585 MeV—the energy range over which coincidence data are taken—changes by only 2–3 %. The off-shell prescription chosen has a much greater effect on the calculated absolute cross sections; the results integrated from 545 to 585 MeV differ by 12–14 %, although neither the shape nor the position of the peak is changed. The ratio of coincidences to singles, however, is much less sensitive to the off-shell prescription, as discussed in Sec. VI.

B. $(e,e'p)$ coincidence data

Missing-energy spectra, $d^3\sigma/d\Omega_e d\Omega_p dE_m$, corrected for individual spectrometer acceptances, were generated at each angle for each of the four targets. The missing energy was calculated using

$$\begin{aligned} \mathbf{p}_r &= \mathbf{p}_{\text{beam}} - \mathbf{p}_e - \mathbf{p}_p \ , \\ \varepsilon &= E_{\text{beam}} + m_{\text{target}} - E_e - E_p \ , \\ E_m &= m_p + \sqrt{\varepsilon^2 - p_r^2} - m_{\text{target}} \ , \end{aligned} \tag{3}$$

where subscripts e and p refer to the scattered electron and proton, respectively, ε is the total energy of the recoiling $A-1$ system and m_{target} is the target mass. Three windows were defined in a two-dimensional histogram of proton time of flight versus momentum; the center window contained real and random coincidences and the windows on either side contained randoms only. The timing resolution was about 2 ns (FWHM). Missing-energy histograms were created for each window and the random spectra were subtracted to yield the real coincidence spectrum. The ratio of real to random coincidences was largest at $\theta_p=58.2°$ where it was ~ 4.5 for carbon and ~ 2 for tantalum. At the largest proton angle, the ratio was ~ 0.3 for all targets.

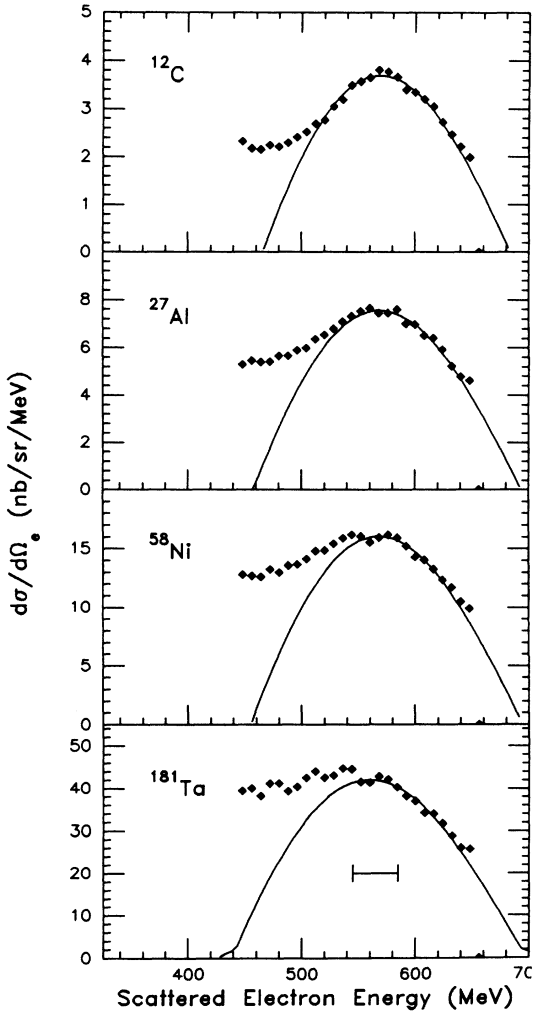

FIG. 1. (e,e') electron spectra for targets ^{12}C, ^{27}Al, ^{58}Ni, and ^{181}Ta, as indicated, together with Fermi-gas fit. The Fermi-gas parameters ε_B (MeV), k_F (MeV/c) are 28, 215 (carbon); 28, 234 (aluminum); 29, 237 (nickel); 37, 264 (tantalum). The range over which coincidence data were taken (545–585 MeV) is indicated.

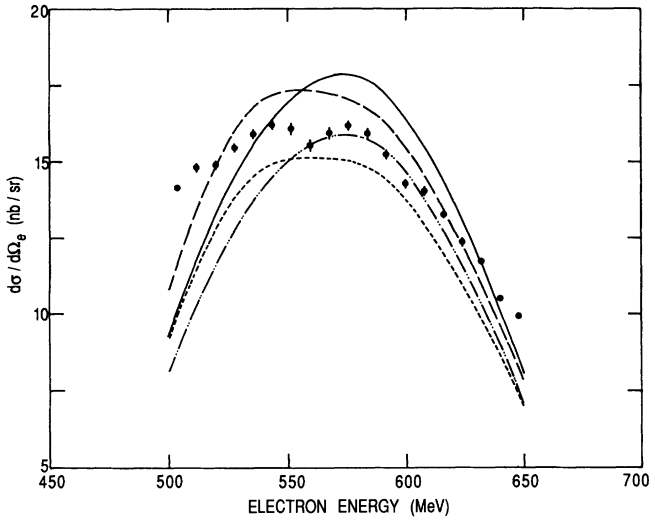

FIG. 2. Comparison of PWIA calculations with (e,e') data for nickel. The dashed curves are results using the state-dependent parametrization of the spectral function for the initial-state (short dashed) or final-state (long dashed) off-shell prescription. The results using the state-independent parametrization of the spectral function and the initial-state (final-state) off-shell prescription are shown as the double-dot-dashed (solid) curves. The coincidence data were taken for the outgoing electron energy range of 545–585 MeV.

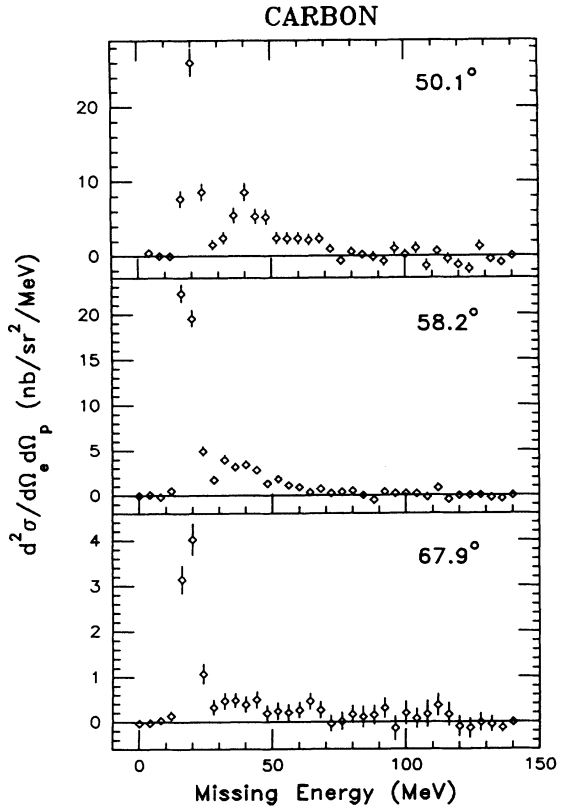

FIG. 3. Missing-energy cross sections for ^{12}C at $\theta_p = 50.1°$, 58.2°, and 67.9° at 779.5 MeV, $\theta_e = 50.4°$. Random coincidences have been subtracted and radiative corrections applied.

The missing-energy spectra for the four targets are shown in Figs. 3–6. Radiative corrections have been applied to these spectra. The radiative corrections are target and angle dependent. The spectra without radiative corrections are shown for tantalum (dashed line in Fig. 6) where the corrections were greatest; the ratio of corrected to uncorrected cross sections (integrated for $0 <$ missing energy < 80 MeV) is ~ 1.1 at 50.1° and ~ 0.9 at the largest angle. Shell structure is apparent; it is most pronounced in the carbon spectra. The missing-energy resolution, as determined from the momentum resolution of the individual spectrometers, was ~ 6 MeV. At the larger angles for the heavier elements, there is significant yield at values of the missing energy greater than 80 MeV. This indicates processes other than quasifree scattering.

The primary results of this experiment are the ratio of coincidences to singles at each of the four proton angles for each target, $\mathcal{R}_{\rm exp}(\theta_p)$. These are obtained by integrat-

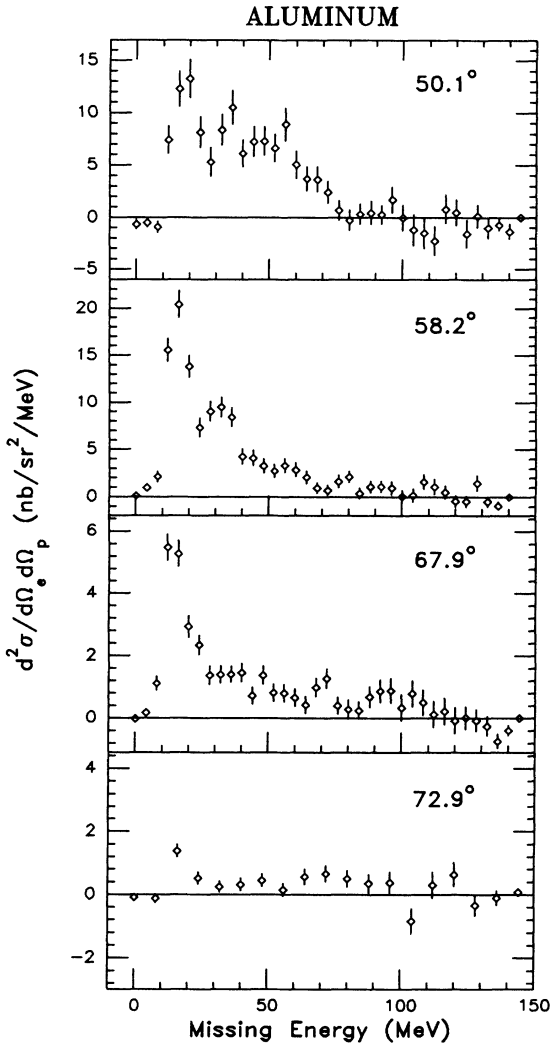

FIG. 4. Missing-energy cross sections for ^{27}Al at $\theta_p = 50.1°$, 58.2°, 67.9°, and 72.9° at 779.5 MeV, and $\theta_e = 50.4°$. Random coincidences have been subtracted and radiative corrections applied.

ing the missing-energy spectra and dividing by the simultaneously measured integrated singles cross section. The radiatively corrected cross sections integrated over the final electron energy range of 545–585 MeV and the entire missing-energy acceptance are presented in Table I and the ratio of coincidences to singles for several ranges of missing-energy integration in Table II.

VI. INTERPRETATION OF $(e,e'p)$ RESULTS

The goal of the present work is to interpret these experimental results in terms of the attenuation of the outgoing proton in the nucleus. The primary assumption is that we are dealing with a quasifree scattering process. This is supported by the comparison of the calculations with the singles data, the proton-electron angular correlations, and the character of the missing-energy spectra. The missing-energy spectra at 50.1° and our understanding of single-particle binding energies suggest that there is single-particle strength at missing energies up to 80 MeV. The yields at higher missing energies on each target have much flatter angular correlations. It seems likely that most of this yield is the result of other processes such as interactions with more than one nucleon or the rescattering of a quasifree proton in the nucleus with significant change of the proton's energy and direction. We have chosen to define the region of missing energy in the range $0 < E_m < 80$ MeV as the quasifree region. Using the results in Table II, the sensitivity of our conclusions to this assumption can be studied.

If there were significant yield from two-body currents in the region of the singles spectrum considered here, then the ratio of coincidence to singles we use will be too low. Rescattering of the protons with small energy and angle loss is strongly inhibited by the Pauli blocking in the final state. Charge-exchange processes [$(e,e'p)$ followed by (p,n) and $(e,e'n)$ followed by (n,p)] will also decrease the measured proton coincidence yield given the dominance of $(e,e'p)$ over $(e,e'n)$. In the framework of a macroscopic measure of attenuation which might be useful for interpreting other experiments, rescattering at small angles and energy losses is unresolvable and is not considered attenuation. With a detailed microscopic

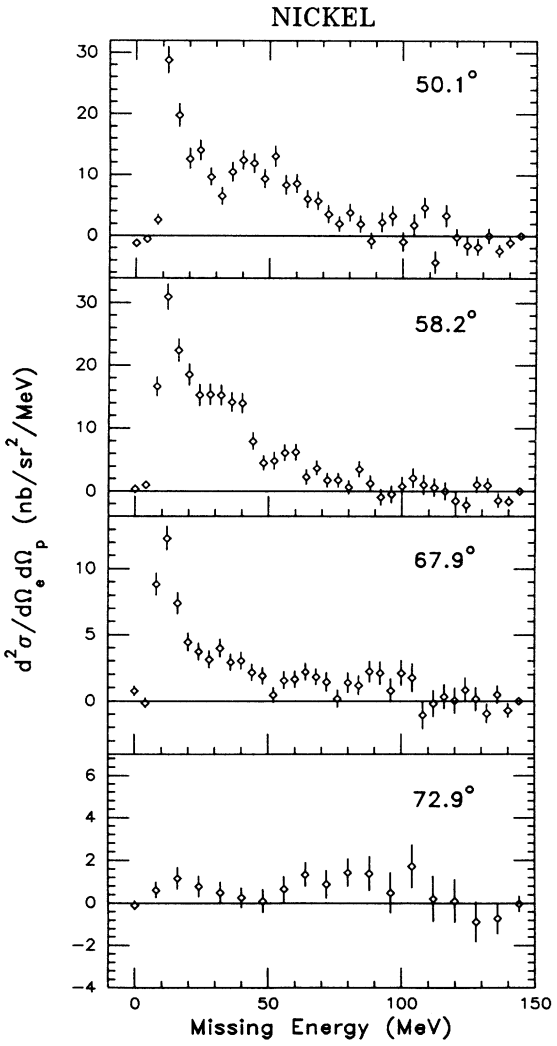

FIG. 5. Same as Fig. 4 except for nickel.

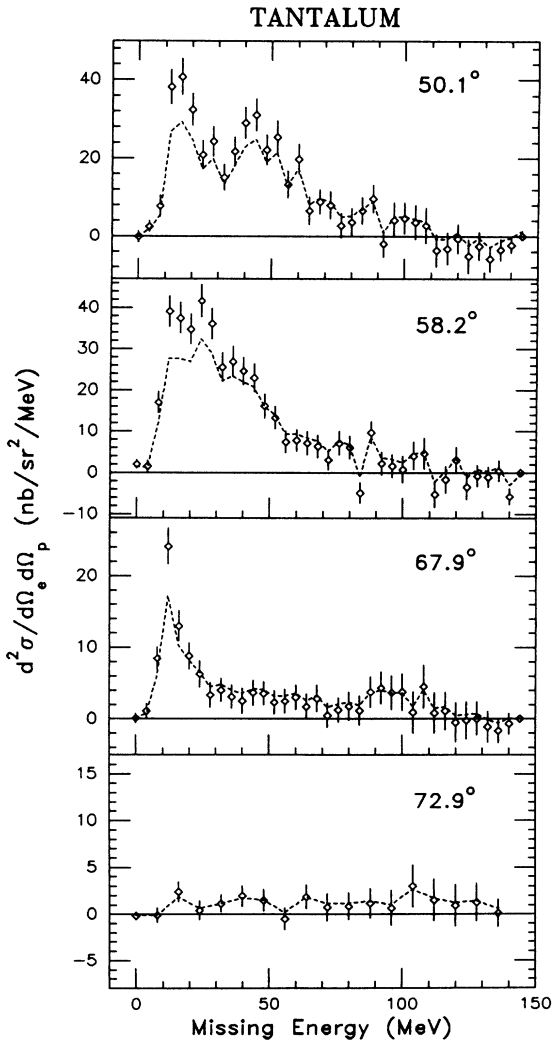

FIG. 6. Same as Fig. 4 except for tantalum. The dashed curves show the spectrum before radiative corrections.

TABLE I. Integrated experimental cross sections with radiative corrections (coincidence cross sections are integrated over the entire missing-energy range).

Target	θ_p (deg)	Coincidence (nb/sr^2) [a]	Singles (nb/sr) [b]
^{12}C	50.1	324±18	137±3
	58.2	279±9	134±2
	67.9	53±5	135±1
^{27}Al	50.1	434±30	278±6
	58.2	483±19	276±4
	67.9	134±8	284±2
	72.9	39±9	298±3
^{58}Ni	50.1	762±36	588±7
	58.2	827±33	589±6
	67.9	295±18	606±5
	72.9	78±24	626±5
^{181}Ta	50.1	1500±89	1572±19
	58.2	1543±73	1564±17
	67.9	468±50	1580±10
	72.9	149±52	1620±13

[a]Only statistical errors are tabulated. Overall systematic errors are estimated to be 6.3%. Relative uncertainties between measurements are estimated to be 2%.

[b]Only statistical errors are tabulated. Overall systematic errors are estimated to be 3.7%. Relative uncertainties between measurements are estimated to be 2%.

model, it might be possible to estimate this contribution, but we have chosen to consider only the measured quantities.

In this section two techniques are considered to relate the measured ratios $\mathcal{R}_{\rm exp}$ to the proton attenuation. In the primary method, PWIA calculations which include no proton attenuation are compared to the experimental results. The agreement in shape indicates that the angular correlation is described by a one-proton knockout mechanism and the ratio of $\mathcal{R}_{\rm exp}$ and $R_{\rm PWIA}$ was used to define the experimental nuclear transmissions, $\mathcal{T}\sim\mathcal{R}_{\rm exp}/\mathcal{R}_{\rm PWIA}$. These results are then compared to a recent calculation which includes the important physical effects: A secondary method is to compare $\mathcal{R}_{\rm exp}$ directly to a DWIA calculation of $\mathcal{R}_{\rm DWIA}$ with a Woods-Saxon imaginary potential. This is in Sec. VI C.

A. PWIA

In the PWIA calculation, there is no provision for proton attenuation, so a comparison of $\mathcal{R}_{\rm exp}$ with $\mathcal{R}_{\rm PWIA}$ was used to define the experimental transmission $\mathcal{T}$. The transmission was defined so as to minimize χ^2:

$$\chi^2=\sum_i\left[\frac{\mathcal{R}_{\rm exp}(\theta_i)-\mathcal{T}R_{\rm PWIA}(\theta_i)}{\Delta\mathcal{R}_{\rm exp}}\right]^2,$$

where θ_i are the four experimental proton angles. Other methods of determining $\mathcal{T}$ were considered, but yielded results that differed by less than 2% from those obtained in this manner. The values of $\mathcal{T}$ differed by less than 1% when determined from $\mathcal{R}_{\rm PWIA}$ calculated using different off-shell cross section prescriptions and by less than $\sim$5% when differing bound-state parametrizations were used. The $\mathcal{R}_{\rm PWIA}$ multiplied by the transmission factors are plotted along with the data in Fig. 7. The $\mathcal{R}_{\rm PWIA}$ calculated using the state-dependent parametrization fit the shape of the data better. The values of $\mathcal{T}$ are presented in Table I for three missing-energy regions with the state-dependent spectral function and one missing-energy region with the state-independent spectral function.

TABLE II. $\mathcal{R}_{\rm exp}=[d^2\sigma(e,e'p)/d\Omega_e d\Omega_p]/[d\sigma(e,e')/d\Omega_e]$, the experimental ratio of coincidences to singles with radiative corrections. The data with no missing-energy cut, and with the missing energy less than 100, 80, and 60 MeV are shown. Only statistical uncertainties are shown. Overall systematic errors are estimated at 3.5%; Systematic relative uncertainties between measurements are estimated at 2%.

Target	θ_p (deg)	No E_m cut	$E_m<100$ MeV	$E_m<80$ MeV	$E_m<60$ MeV
^{12}C	50.1	2.36±0.14	2.45±0.13	2.44±0.13	2.28±0.12
	58.2	2.09±0.07	2.09±0.07	2.08±0.07	2.02±0.06
	67.9	0.39±0.04	0.38±0.03	0.36±0.03	0.34±0.02
^{27}Al	50.1	1.56±0.11	1.68±0.10	1.64±0.09	1.50±0.08
	58.2	1.75±0.07	1.71±0.07	1.66±0.06	1.56±0.06
	67.9	0.47±0.03	0.47±0.02	0.43±0.02	0.38±0.02
	72.9	0.13±0.03	0.14±0.02	0.12±0.02	0.08±0.01
^{58}Ni	50.1	1.30±0.06	1.31±0.05	1.27±0.05	1.13±0.04
	58.2	1.40±0.06	1.41±0.05	1.38±0.05	1.31±0.04
	67.9	0.49±0.03	0.48±0.02	0.43±0.02	0.38±0.02
	72.9	0.12±0.04	0.13±0.03	0.10±0.02	0.06±0.02
^{181}Ta	50.1	0.95±0.06	1.01±0.05	0.95±0.04	0.87±0.04
	58.2	0.99±0.05	1.00±0.04	0.98±0.04	0.90±0.03
	67.9	0.30±0.03	0.29±0.02	0.25±0.02	0.23±0.02
	72.9	0.09±0.03	0.06±0.02	0.05±0.02	0.03±0.01

Given the simultaneous measurement of singles and coincidence data the only source of systematic uncertainty in $\mathcal{R}_{exp}$ is the uncertainty in the BIGBITE normalization. The statistical error in the transmission quoted in the table is determined from the amount of variation of the transmission which increases χ^2 by one unit. Other sources of uncertainty are the effects of the differing off-shell prescriptions (2%), the choice of the bound-state single-particle potential (5%) and the uncertainty introduced in the choice of the missing-energy cut (estimated at 3%). The state-dependent single-particle potentials are to be preferred from a theoretical point of view and provide a better overall fit to the shape of the angular correlation, so the tabulated transmissions are determined with these spectral functions and the overall systematic uncertainty is estimated to be 5%. The uncertainty in the OHIPS normalizations, including the uncertainty in the radiative corrections, cancels out in the transmission determination. It is very difficult to quantitatively estimate the validity of the assumption of the quasifree scattering mechanism and this has not been included in the systematic errors.

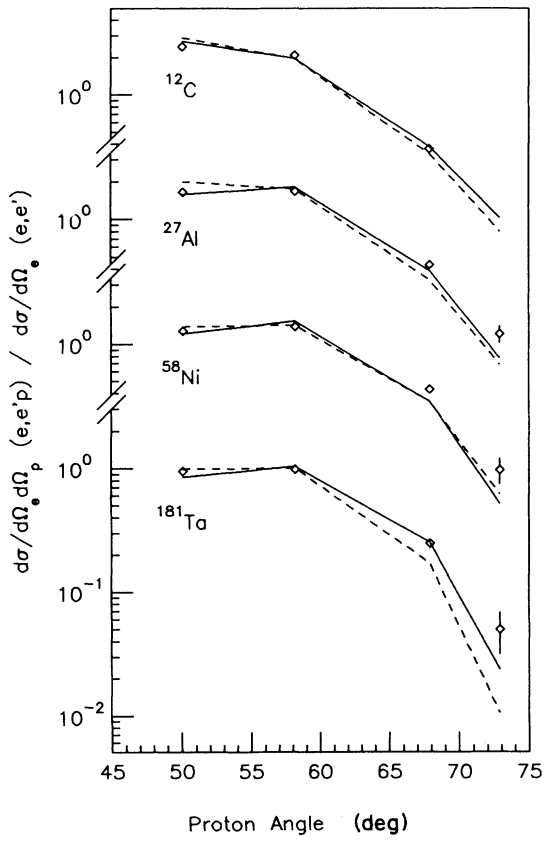

FIG. 7. Ratio of coincidence yield integrated over a missing-energy range of 0–80 MeV to integrated singles yield compared to the PWIA results multiplied by the experimental transmissions that best fit the data. Curves show PWIA results using initial off-shell prescription and state-dependent (solid) and state-independent (dashed) parametrizations.

B. Calculation of the transmission

In the first Brief Report of this work [29], the preliminary results were compared with a classical attenuation calculation with an ansatz for the density dependence of the nucleon-nucleon interaction in the medium. The present results are consistent with those of Ref. [29], which yielded a mean free path of ~5 fm. Recently Pandharipande and Pieper [30] have proposed a simple relation between the nucleon-nucleon cross sections in vacuum and nuclear matter. This is used with the local density approximation and the correlated Glauber approximation to calculate the transparency in $(e,e'p)$ reactions. The ingredients of these calculations are as follows.

(a) The absorption of a proton in infinite nuclear matter was calculated for *N-N* scattering assuming a filled Fermi sea for a given density and taking into account the energy dependence and angular distribution of the *N-N* cross sections. (The forward-backward peaking of the *p-n* scattering increases the Pauli suppression substantially.)

(b) Realistic nuclear density distributions were obtained by unfolding the proton charge distribution from nuclear charge distributions measured in electron elastic scattering. The neutron density was assumed to be proportional to the proton density.

(c) The experimental *p-p* and *p-n* cross sections were used as parametrized by a phase-shift analysis.

(d) The transparency of a nucleus was computed by folding the nuclear-matter results with the nuclear density.

(e) The two-body *p-p* and *p-n* correlations as calculated in nuclear matter are included. This is a significant effect because the struck nucleon cannot reinteract with itself and because the repulsive core of the *N-N* interaction creates a hole around the struck nucleon.

The imaginary part of the optical potential calculated in this fashion is in good agreement with the results of correlated basis theory [31] and empirical values obtained from proton-nucleus scattering.

There are no free parameters in this calculation. In Fig. 8, the results of various components of this calculation are compared to the transmissions of Table III. The combined statistical and experimental error bars are shown. The solid curve is the result of the full calculation. The dotted curve shows the calculation with just the free *N-N* cross sections. As other ingredients are added (Pauli blocking, dashed curve; density-dependent effects of the *N-N* cross section, dot-dashed curve; two-nucleon correlation, solid curve) the results approach the experimental data. As Pandharipande and Pieper show, the two-nucleon correlations have a significant impact on the transmission.

C. DWIA

DWIA calculations provide a direct comparison of the transmission with an optical potential. However, they do not include significant physical effects such as the two-nucleon correlations discussed above. Given the difficulty in including a spin-orbit potential in a factorized DWIA calculation, the calculations presented here

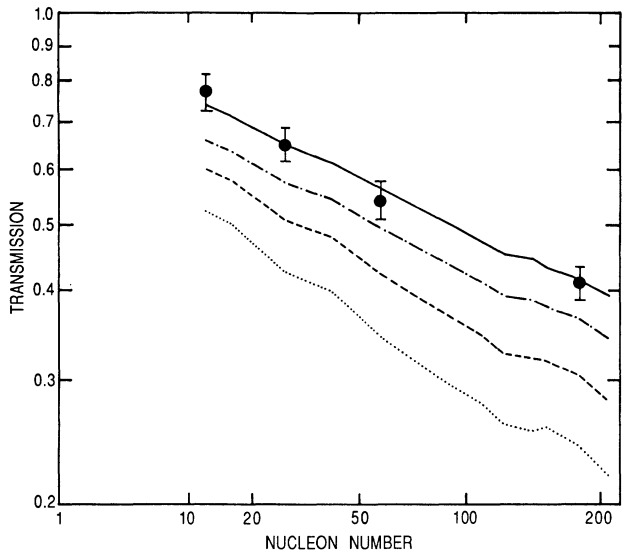

FIG. 8. The experimental transmissions (on a logarithmic scale) from Table III for a missing-energy range of 0–80 MeV vs nucleon number of the target nucleus (on a cube-root scale) are shown including the systematic errors. The lines represent the calculations of Ref. [30] described in Sec. VI B. The solid curve is the result of the full calculation. The other curves are for the free *N-N* cross sections (dotted), adding Pauli blocking (dashed) and adding density-dependent effects of the *N-N* cross section (dot-dashed).

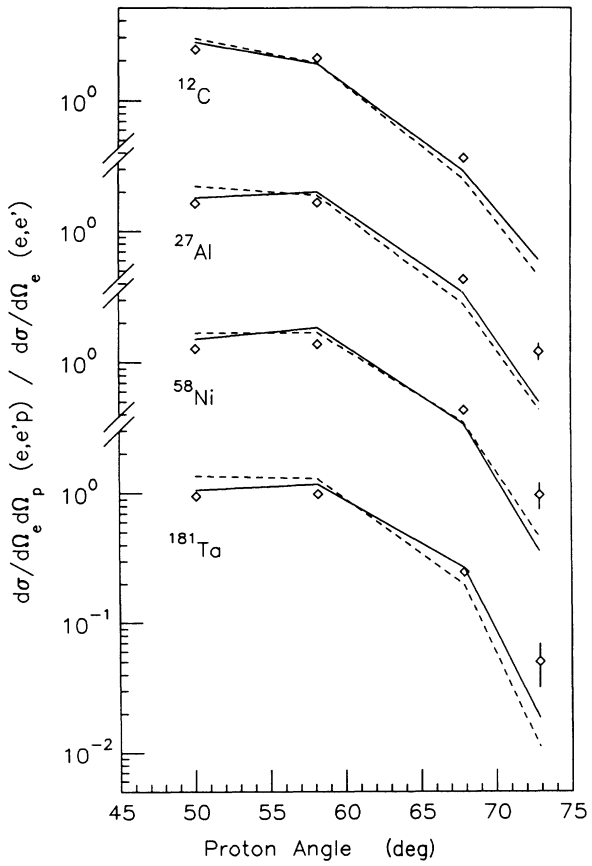

FIG. 9. Ratio of coincidence yield integrated over a missing-energy range of 0–80 MeV to integrated singles yield compared to the DWIA results. Curves show DWIA results using initial off-shell prescription and state-dependent (solid) and state-independent (dashed) parametrizations.

should only be regarded as schematic. As is seen in Fig. 9, the shapes of the DWIA angular correlations are similar to the PWIA and there is a significant dependence on the choice of spectral function. (The dependence on the choice of off-shell prescription was less than 5%.) For ^{58}Ni and ^{181}Ta, the calculated cross sections are too large at the angles where the yield is the highest and indications are that the volume imaginary potential should be increased by ~ 1.5, roughly consistent with the mean free path implied by Ref. [30]. Given the schematic nature of the calculations which were not constrained to the proton elastic scattering data, we did not attempt to find a "best-fit" imaginary potential.

VII. CONCLUSIONS

In this experiment the ratio of the integrated missing-energy coincidence $(e,e'p)$ cross sections to the integrated (e,e') cross sections was measured for several targets ($A = 12$–181) as a function of proton angle for an average proton kinetic energy of 180 MeV. This is the first experiment to perform such a broad integration in the quasifree region for this regime of proton energies. The purpose of the experiment was to obtain a macroscopic measure of the proton attenuation.

A comparison of the experimental ratio of coincidences to singles with those calculated in the PWIA provided a measure of the transmission of protons in this reaction. The general features of the singles and coincidence data support the interpretation of the reaction as primarily quasifree $(e,e'p)$ scattering. We observe that almost 80% of the protons emerge in the quasifree cone from the carbon target and about 40% from tantalum.

For the heavier targets at the larger angles, there is considerable yield at missing energies greater than 80 MeV, the limit considered here for quasifree scattering. It is likely that a significant contribution to this yield is from multinucleon currents or proton rescattering and charge exchange. One estimate of the rescattering and charge-exchange contributions suggests that these processes contribute less than 0.02 to the results of Table III in the missing-energy range of 0 to 80 MeV [13] and are thus within the systematic errors. Several authors have begun to study this problem; for instance, Takaki [32] has considered nucleon rescattering in the dip region and Van Orden and Donnelly [33] have considered meson-exchange currents (MEC) for the singles case. Correcting for MEC contributions to the singles spectra might imply slightly increased proton transmissions. A complete study of the entire range of missing energy would help ascertain the validity of our assumption of a quasifree reaction mechanism. Our results are not particularly sensitive to the limits of integration of missing energy. We have concentrated on the experiment results and the con-

TABLE III. Transmissions calculated using R_{PWIA} using the initial off-shell prescription.

Target	No cut	State dependent $E_m < 80$ MeV	State dependent $E_m < 60$ MeV	State independent $E_m < 80$ MeV	Uncertainties ±statistical	Uncertainties ±systematic
^{12}C	0.77	0.77	0.73	0.76	±0.02	±0.04
^{27}Al	0.67	0.65	0.60	0.64	±0.02	±0.03
^{58}Ni	0.55	0.54	0.50	0.53	±0.01	±0.03
^{181}Ta	0.42	0.41	0.38	0.38	±0.01	±0.02

text of a macroscopic definition of the nuclear attenuation.

DWIA calculations with a volume optical potential which implies a relatively long ($\sim$6 fm) mean free path provided too little attenuation for all but the lightest target considered here.

The transmissions are compared with a calculation of Pandharipande and Pieper in a companion paper and the agreement is good. The calculated increase in transmission from the "free plus Pauli corrected" transmission is due to the density dependence of the *N-N* interaction and the two-nucleon correlations. It has been noted that this latter mechanism will also be important in higher energy studied of hadron propagation in nuclei such as searches for "color transparency" or other QCD-inspired formation-time effects [34].

ACKNOWLEDGMENTS

We thank V.R. Pandharipande and S.C. Pieper for many useful discussions during this work and for the calculations relating directly to our results. We thank the staff of the Bates Linear Accelerator Center for their support in carrying out this experiment. This work was supported at Argonne National Laboratory by the Department of Energy, Nuclear Physics Division, under Contract No. W-31-109-ENG-38, Northwestern University by the National Science Foundation under Grant No. PHY-8608247, Massachusetts Institute of Technology by the Department of Energy under Contract No. DE-AC02-76ER03069, and the University of Maryland by the National Science Foundation under Contract No. PHY-8615512.

[1] K. Kikuchi and M. Kawai, *Nuclear Matter and Nuclear Reactions* (North-Holland, Amsterdam, 1968), p. 35.
[2] M. T. Collins and J. J. Griffin, Nucl. Phys. **A348**, 63 (1980).
[3] P. Schwandt, *The Interaction Between Medium Energy Nucleons in Nuclei,* edited by H. O. Meyer (American Institute of Physics, New York, 1982), p. 89.
[4] H. O. Meyer and P. Schwandt, Phys. Lett. **107B**, 353 (1981).
[5] J.-P. Jeukenne, A. Lejeunne, and C. Mahaux, Phys. Rep. **25**, 83 (1976); J.-P. Jeukenne, A. Lejeune, and C. Mahaux, *Proceedings of the International Conference on the* Interactions of Neutrons with Nuclei, edited by E. Sheldon (National Technical Information Service, Springfield, VA, 1976), p. 451.
[6] H. Feshbach, Annu. Rev. Nucl. Sci. **8**, 49 (1958).
[7] J. W. Negele and K. Yazaki, Phys. Rev. Lett. **47**, 71 (1981).
[8] S. Fantoni, B. L. Friman, and V. R. Pandharipande, Phys. Lett. **104B**, 89 (1981).
[9] P. U. Renberg, D. F. Measday, M. Pepin, P. Schwaller, B. Favier, and C. Richard-Serre, Nucl. Phys. **A183**, 81 (1972).
[10] R. Dymarz and T. Kohmura, Phys. Lett. **124B**, 446 (1983).
[11] J. P. Schiffer, Nucl. Phys. **A335**, 339 (1980).
[12] J. G. Cramer and R. M. DeVries, Phys. Rev. C **22**, 91 (1980).
[13] G. Garino, Ph.D. Thesis, Northwestern University, 1990.
[14] W. Bertozzi, M. V. Hynes, C. P. Sargent, C. Creswell, P. C. Dunn, A. Hirsch, M. Leitch, B. Norum, F. N. Rad, and T. Sasanuma, Nucl. Instrum. Methods **141**, 457 (1977).
[15] *Introduction to Q* (LAMPF Report MP-1-3401-3, 1986); *Q Programmer's Information Manual* (LAMPF Report MP-1-3401-5, 1986).
[16] W. Bertozzi, M. V. Hines, C. P. Sargent, W. Turchinetz, and C. Williamson, Nucl. Instrum. Methods **162**, 211 (1979).
[17] W. Reuter, G. Fricke, K. Merle, and H. Miska, Phys. Rev. C **26**, 806 (1982).
[18] L. W. Mo and Y. S. Tsai, Rev. Mod. Phys. **41**, 205 (1969).
[19] Y. S. Tsai, *Proceedings of Nucleon Structure Conference at Stanford,* edited by R. Hofstadter and L. I. Schiff (Stanford University Press, Stanford, CA, 1964) p. 221.
[20] Y. S. Tsai, Report SLAC-PUB-848, January 1971.
[21] C. Marchand, Ph.D. Thesis, University of Paris-Sud, 1987.
[22] E. J. Moniz, Phys. Rev. **184**, 1154 (1969).
[23] S. Frullani and J. Mougey, Adv. Nucl. Phys. **14**, 1 (1984).
[24] T. de Forrest, Jr., Nucl. Phys. **A392**, 232 (1983).
[25] N. S. Chant and P. G. Roos, Phys. Rev. C **27**, 1060 (1983); N. S. Chant, program THREEDEE (private communication).
[26] H. de Vries, C. W. de Jager, and C. de Vries, At. Data Nucl. Data Tables, **36**, 495 (1987).
[27] S. Boffi, C. Giusti, F. D. Pacati, and S. Frullani, Nucl. Phys. **A319**, 461 (1979).
[28] A. Nadasen, P. Schwandt, P. P. Singh, W. W. Jacobs, A. D. Bacher, P. T. Debevec, M. D. Kaitchuck, and J. T. Meek, Phys. Rev. C **23**, 1023 (1981).
[29] D. F. Geesaman *et al.*, Phys. Rev. Lett. **63**, 734 (1989).
[30] V. R. Pandharipande and S. C. Pieper, Phys. Rev. C **45**, 791 (1992), following paper.
[31] S. Fantoni, B. L. Friman, and V. R. Pandharipande, Nucl. Phys. **A386**, 1 (1982); **A391**, 51 (1983).
[32] T. Takaki, Phys. Rev. C **39**, 359 (1989).
[33] J. W. Van Orden and T. W. Donnelly, Ann. Phys. (N.Y.) **131**, 451 (1981).
[34] O. Benhar, A. Fabrocini, S. Fantoni, V. R. Pandharipande, and I. Sick, unpublished.